Single-atom point source for electrons: Field-emission resonance tunneling in scanning tunneling microscopy

J. W. Gadzuk
National Institute of Standards and Technology, Gaithersburg, Maryland 20899
(Received 19 November 1992)

Many years ago spectroscopic evidence based on a single-electron process, namely, field-emission resonance tunneling, was reported showing the electronic structure of single atoms adsorbed on metal surfaces. Huge enhancements in the highly collimated tunneling current through the virtual states of the adparticle made the single-atom spectroscopy feasible when the field-emission spectrometer was operated in the "probe-hole mode." A related effect is currently popular in today's scanning tunneling microscopy and also in nanometer-cluster spectroscopy. The phenomenology and theory of the effect is presented and the current activity is considered in light of what has been uncovered in the field-emission work.

I. INTRODUCTION

Motivated by the experimental work of Fink in which scanning-tunneling-microscope (STM) tips were used in a field-emission mode as a "point source" to produce narrow, collimated electron beams,[1] Lang, Yacoby, and Imry have analyzed "the microscopic aspects of field emission from [such] tips on which the primary emission source is a single atom."[2] Their model for this problem is "one used earlier to study aspects of current flow in the STM,[3] two planar metallic electrodes with a bias between them, with an adsorbed atom kept fixed at its zero-field equilibrium distance on one of the electrodes." Calculations based on this model can predict a relatively focused, high-current beam with a narrow energy distribution, in agreement with experimental studies. These results have then been interpreted physically in terms of "channel filtering by an adiabatic constriction."

The purpose of the present paper is to suggest some possible connections between this effect and the phenomenon of field-emission resonance tunneling (FERT) within the "probe-hole" mode, predicted,[4] observed,[5] and developed[6] into the first viable single-electron spectroscopy of adsorbed atoms and/or molecules more than 20 years ago. It will be seen that the descriptive theory of FERT could provide a helpful complement to present-day modeling of STM phenomena just as it has in the interpretation of recent FERT experiments in which the discrete electron states of Au clusters supported on W(110) field-emission tips[7(a)] and single W atoms on nanoprotrusion tips [7(b)] have been observed. Furthermore, it could be enlightening to consider single-atom tunneling from a historical perspective as this is an aspect of STM research that has at times been overlooked.[8] In order to achieve these goals, a brief review of the relevant field-emission phenomenology is given. Then the theory is reworked into a form that addresses the issues of constricted and focused point-source electron emission, currently under examination in STM. We conclude with some final commentary and observations.

II. FIELD-EMISSION PHENOMENOLOGY

A. General

The field-emission microscope (FEM) and its derivative spectroscopies are based on the fact that a modest potential ($\sim 1-3$ keV) applied between a sharpened conducting tip (radius ~ 100 nm) and a flat or concentric spherical electrode, positioned a macroscopic distance ($\sim 1-10$ cm) away, will result in an electric field at the emitter surface whose strength is $F \sim 0.1-1.0$ V/Å. If the sign of the potential is such that the surface barrier for electrons is "bent over," then electrons from the tip can tunnel through the "triangle barrier" $V_B(z) = +\theta(z)(E_F+\phi-eFz)$, where z is the coordinate normal to the surface which, on a scale of Angstroms, looks flat, not spherical. Consequently, the problem is well modeled as a degenerate three-dimensional electron gas confined by a tunnel barrier that varies only in one Cartesian coordinate. The classical turning points for an electron with "normal" kinetic energy $=W$ are at $z=0$ and $z=s_T(W)=(\phi+E_F-W)eF$, where ϕ is the work function and E_F the Fermi energy, as shown in Fig. 1(a). Typically, the outer turning point of a Fermi-level elec-

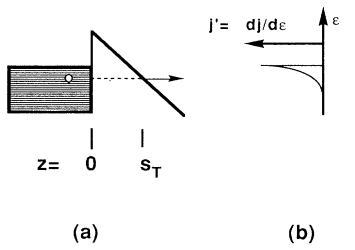

FIG. 1. (a) Energy-level/potential-energy diagram for field emission from a metal surface. For the tunneling electron depicted by the dashed line, the triangle barrier, uncorrected for image forces, extends between $z=0$ and $z=s_T$. (b) Zero-temperature total energy distribution of field-emitted electrons given by Eq. (1).

tron is $s_T \sim 15-20$ Å. The field-emission theory is easily worked out analytically[6,9] with the triangle barrier in contrast to the more realistic "image-potential-rounded" barrier, which requires some additional numerical considerations that do not affect any of the physics points to be made here.[9] For the sake of clarity we will consider only the triangle barrier.

A subtle point involving length scales, electron optics, and focusing arises in the mixed Cartesian geometry of the tunneling process and the spherical geometry of the actual FEM. On an atomic or nanometer level, the tunneling barrier varies only in the z direction (ignoring small effects due to surface corrugation[10]) and thus the distinction between normal and transverse momentum or energy is maintained in the tunneling or field-emission process. However, the macroscopic geometry of the FEM provides an angular-momentum-conserving radial accelerating field that has at least two important consequences. First, note that the initial angular distribution of the field-emitted electrons, as established by the nanometer-scale tunneling process, is not distorted by the macroscopic electron optics. Nonetheless, mixing of initial transverse and normal momenta of the emitted electron by the radial field at macroscopic distances from the surface obscures this fact. Second, due to this radial field effect, an electron energy analyzer connected to a field-emission source measures a total, not normal energy distribution, as originally recognized by Young[11] and further discussed at length by Gadzuk and Plummer.[6] The standard theory[6,11] leads to an exponentially decreasing electron total-energy distribution (TED) with a high-energy Fermi edge,

$$j_0' = dj_0/d\epsilon = (J_0/d)\exp(\epsilon/d) f(\epsilon) , \tag{1a}$$

where

$$J_0 = (\mathrm{med}^2/2\pi^2\hbar^3)\exp(-c) , \tag{1b}$$

$$c = (2m/\hbar^2)^{1/2} \times (4\phi^{3/2}/eF) = 0.683 \times (\phi^{3/2}/F) , \tag{1c}$$

and

$$1/d = (2m/\hbar^2)^{1/2} \times (2\phi^{1/2}/eF) = 1.025 \times (\phi^{1/2}/F)\mathrm{eV}^{-1} , \tag{1d}$$

with $\epsilon = \epsilon_f - E_F$ the electron energy with respect to the Fermi energy, J_0 the total (Fowler-Nordheim) current, $f(\epsilon)$ the Fermi function, and ϕ and F given in eV and V/Å, respectively.[12] The zero-temperature distribution shown schematically in Fig. 1(b), has a full width at half maximum given by $\Delta\epsilon_{1/2} \simeq 0.69d$ which is ~ 0.1 eV for typical field-emission conditions.

B. Single-atom emission

If a fluorescent screen is introduced behind the accelerating electrode, then a projection of the field-emission tip can be imaged with a spatial resolution of a few nanometers. Contrast in the image is due to variations in electron emission across the tip surface, historically attributed to variations in work function. Furthermore, a "small" hole, called a probe hole, can be made in the screen so that electron emission from a surface region composed of $\sim 15-30$ atoms passes through the hole and then into an energy analyzer, thus facilitating electron spectroscopy studies. Deflection grids are used to position the emitted current from a chosen portion of the surface over the probe hole.

When a single "quantum particle" (atom, molecule, or cluster[7]) is adsorbed onto that portion of the surface emitting through the probe hole, and if the adsorbate has an electron quasibound state near the Fermi level of the tip, then a substantial increase in the probe-hole current can occur due to resonance-tunneling enhancement through the adsorbate. This phenomenon was first observed by Clark and Young[5(a)] in their study of Sr adsorption on W field-emission tips and their key result is reproduced in Fig. 2. Shown here is the total field-emission current through a probe hole as a function of time after a Sr evaporation source has been turned on. The arrival of a single Sr atom on the emitting area results in a step-function increase in the total current. Upon adsorption of a single atom, the source can be turned off and an energy distribution of the probe-hole current obtained. The structure in the observed TED reflects the local density of electronic states of the adsorbate, and led to an unambiguous electron spectroscopy of single adsorbed atoms.[5,13]

The physical origin of the effect can be understood from the FERT-model potential-energy diagram and wave functions shown in Fig. 3. The field-emission configuration illustrated earlier in Fig. 1(a) is here augmented by a potential well of width $2w$ centered at $z = s$, representing the adsorbate characterized by a discrete level broadened into a local density of states defined as $\rho_a(\epsilon)$. Enhanced tunneling occurs for those tip states ψ_m whose energy is resonant with $\rho_a(\epsilon)$, in which case the sequential process of $\psi_m \rightarrow \psi_a$ and then $\psi_a \rightarrow \psi_f$ occurs with much greater probability (by factors as large as $\sim 10^2-10^4$) than for direct $\psi_m \rightarrow \psi_f$ tunneling. It is this magnification which is responsible for the collimated emission from the single adsorbate rising far above the background emission from other parts of the field emitter surface.

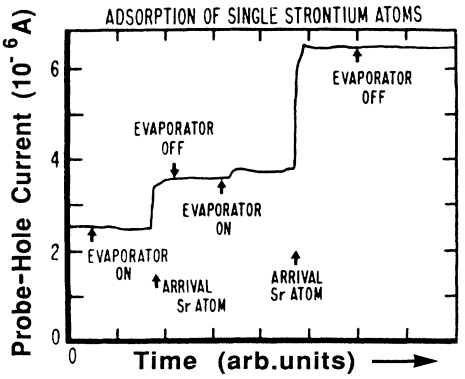

FIG. 2. Probe-hole current vs time as the strontium source is switched on and off. The step increase in current occurs when a single Sr atom arrives upon the surface being viewed [based on Clark and Young, Ref. 5(a); see also Ref. 6].

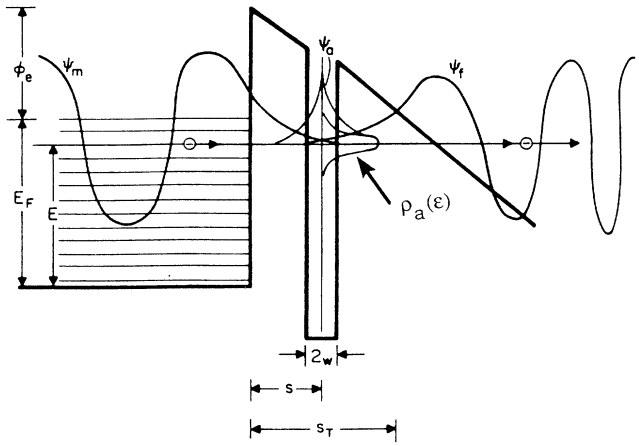

FIG. 3. Schematic model showing the idealized potentials relevant in field-emission resonance tunneling. The electron wave functions are ψ_m, the unperturbed metal function; ψ_a, the localized adsorbate resonance function; and ψ_f, the emitted electron function. The adatom centered at $z=s$, with diameter equal to $2w$, shows a Lorentzian-like local density of states labeled ρ_a.

In considering the spectroscopic characteristics of emission from the composite surface, it is most informative to measure and display the ratio of the change in TED to the original TED, $\Delta j'(\epsilon)/j_0'(\epsilon)$ vs ϵ, since in this form the dominating but uninteresting exponential in Eq. (1) is canceled out. For an adsorbate satisfying the reasonable condition $s \ll s_T$, "standard" theory[6] has also shown that this ratio, for emission from the adsorbate-covered surface area, is

$$\Delta j'(\epsilon)/j_0'(\epsilon) \simeq \sum_a [\rho_a(\epsilon)/\rho_m(\epsilon)] \exp[+2\kappa(s+w_a)] , \tag{2}$$

where the summation is over the adsorbate states labeled by the set of quantum numbers $\{a\}$, $\rho_a(\epsilon)$ is the adsorbate density of states derived from state a, usually represented by a Lorentzian

$$\rho_a(\epsilon) \equiv \frac{1}{\pi} \frac{\Delta_a}{(\epsilon-\epsilon_a)^2+\Delta_a^2} , \tag{3}$$

with ϵ_a and Δ_a, the resonance position and width, depending upon the particular state, $\rho_m(\epsilon)$ the substrate density of states, w_a the effective "radius" of the a'th state, and $\kappa \simeq [(2m/\hbar^2)(\phi_e-\epsilon)]^{1/2}$. The structure in the TED that provides the spectroscopic information arises from $\rho_a(\epsilon)$. The enhancement is mainly a consequence of the fact that the rate-limiting step is tunneling from the adsorbate to vacuum, through a reduced barrier compared to direct metal-vacuum tunneling. This enhancement is accounted for by the exponential factor in Eq. (2). When comparing with actual data, one must also account for the "background current" from the noncovered portion of the emitter that contributes to the probe-hole current, usually by introducing a multiplicative geometrical factor $\sim A_{\rm ads}/A_{\rm tot} \sim 0.05$–$0.1$ into Eq. (2), where $A_{\rm ads(tot)}$ is the effective area of the adsorbate (total) emitting surface.

As a final aside, one should note that the properties of the resonance state such as the width, depth, location of the potential well, and consequently the eigenvalues ϵ_a, wave functions ψ_a (and as a result, the geometrical extent), and the level broadening impose constraints on the resonant tunneling through the adparticle or constricted channel; it is here that the similarities with current STM and mesoscopic systems exist. This will be detailed in the next section.

III. COLLIMATED POINT SOURCE

A. General resonance tunneling theory

Almost all theories of resonant tunneling are based on some type of Golden Rule or scattering-theory formulation in which the tunneling process is characterized by the sum of a nonresonant plus a resonance matrix element[14–16]

$$M_T \simeq \langle F|O_T|M\rangle + \sum_a \frac{\langle F|O_T|A\rangle\langle A|O_T|M\rangle}{\epsilon-\epsilon_a-i\Delta_a} , \tag{4}$$

where $|M\rangle$, $|A\rangle$, and $|F\rangle$ are the metal, adsorbate, and free states represented by the configuration-space wave functions in Fig. 3 and O_T is some operator whose specification here is not yet crucial,[17] but which allows for transfer of electrons between the states in the three separated spatial regions of the emitter ($z<0$), the adsorbate or quantum well ($z \simeq s \pm w_a$), and free space ($z > s_T$). It is not unreasonable to assume separable free and metal states

$$|F\rangle = e^{i\mathbf{k}_\parallel'\cdot\rho} f(z;\mathbf{k}_\parallel',\epsilon) \tag{5a}$$

and

$$|M\rangle = e^{i\mathbf{k}_\parallel\cdot\rho} m(z;\mathbf{k}_\parallel,\epsilon) \tag{5b}$$

and a transfer operator $O_T = O_z(z)$ which is a function of the normal coordinate and/or momentum only.

The nonresonant field-emission current density can be described by the Golden-Rule transition rate

$$w_{m\to f} = (2\pi/\hbar) \sum_f |\langle F|O_T|M\rangle|^2 \delta(\epsilon_f-\epsilon_m) \tag{6}$$

summed over all occupied initial states (including spin), hence,

$$j_0 = 2e \sum_m f(\epsilon_m) w_{m\to f} . \tag{7}$$

With wave functions given by Eq. (5) the modulus-squared tunneling matrix element becomes

$$|\langle F|O_T|M\rangle|^2 = (2\pi)^2 \delta^{(2)}(\mathbf{k}_\parallel-\mathbf{k}_\parallel') |\langle f_z|O_z|m_z\rangle|^2 . \tag{8}$$

Note that the conservation of $\mathbf{k}_\parallel$ selection rule in the uncorrugated surface tunneling process has appeared naturally in Eq. (8) as a consequence of Eq. (5) and the fact that there are no transverse forces throughout the tunneling process when O_T is a function of z only.

Proceeding with the substitution

$$\sum_f \rightarrow \sum_{\mathbf{k}'_\parallel} \int \rho_f d\epsilon_f \ ,$$

where ρ_f is the right-hand vacuum density of states for fixed $\mathbf{k}'_\parallel$ (and similarly for the initial-state m sum), Eqs. (6)–(8) lead to

$$j_0 = \frac{4\pi e}{\hbar} \sum_{\mathbf{k}_\parallel} \int_{-\infty}^{\infty} d\epsilon_f f(\epsilon_f) \rho_f \rho_m |\langle f_z | O_z | m_z \rangle|^2 \ . \quad (9)$$

Invoking Harrison's WKB approximation,[18] the transfer Hamiltonian[17] matrix element is

$$4\pi^2 \rho_f \rho_m |\langle f_z | O_z | m_z \rangle|^2 = \exp\left[-2\int_0^{s_T} |k(z)| dz\right] = D_0(W) \ , \quad (10)$$

which is a measure of the z-dependent exponential decay of the wave-function overlap. The total-energy distribution of the emitted current implied by Eqs. (9) and (10) is

$$dj_0/d\epsilon_f = (e/\pi\hbar) f(\epsilon_f) \sum_{\mathbf{k}_\parallel} D_0(W) \ , \quad (11)$$

where $k(z) = \{(2m/\hbar^2)[V(z) - W]\}^{1/2}$ and $W = \epsilon_f - \hbar^2 k_\parallel^2 / 2m$ is the so-called normal energy.[11,19]

Finally, since at constant total energy,

$$\sum_{\mathbf{k}_\parallel} \rightarrow \int_0^{\epsilon_f} (m/2\pi\hbar^2) dW \ ,$$

Equation (11) evaluated with $D_0(W) = \exp[-c + (W - E_F)/d]$ yields[20] $dj_0/d\epsilon_f = (J_0/d) f(\epsilon) \exp(\epsilon/d)$, the standard result[6] given by Eq. (1).

When resonance tunneling is possible, the tunneling rate is dominated by the resonant matrix element in Eq. (4). For (energetically) nonoverlapping resonances, the field-emission current is now determined by the electron occupation decay rate out of the adatom immersed in the field which, from Eq. (4) and the golden rule, is

$$j_{\text{res}} = \left[\frac{4\pi e}{\hbar}\right] \sum_{a,f,m} f(\epsilon_m) \frac{|\langle F|O_T|A\rangle|^2 |\langle A|O_T|M\rangle|^2}{(\epsilon_m - \epsilon_a)^2 + \Delta_a^2} \times \delta(\epsilon_f - \epsilon_m) \ . \quad (12)$$

Noting that the adsorbate-level width due to coupling with the surface is[21]

$$\Delta_a(\epsilon) = \pi \sum_m |\langle A|O_T|M\rangle|^2 \delta(\epsilon - \epsilon_m) \ ,$$

Eqs. (3) and (12) can be turned into

$$j_{\text{res}} = \left[\frac{4\pi e}{\hbar}\right] \sum_{a,f} f(\epsilon_f) \rho_a(\epsilon_f) |\langle F|O_T|A\rangle|^2 \ , \quad (13)$$

which has an interesting interpretation when the adatom or resonant well is close enough to the surface so that atom-to-metal tunneling is very fast on the time scale set by atom-to-free-space tunneling. The decay rate implied by Eq. (13) is basically the atomic field-ionization rate considered initially by Oppenheimer.[17] The principle difference between field-ionization and resonant-tunneling situations is that in the latter, the electronic occupation of the atom is maintained at the steady-state equilibrium value due to strong coupling with the electron reservoir. When all things are considered, it is seen that the main role of the small-radius (~ 1000 Å) substrate tip that distinguishes resonant field emission from free-space field ionization is to serve as a fast, unlimited electron source and to provide the surface electrodynamic boundary conditions that make attainment of the high electric fields possible.[22] In this way, the phenomenon of field-emission resonance tunneling has exploited the common mechanism of free-atom field ionization and mesoscopic solid-state-constricted conductance through single atoms.

To proceed, some specifics and/or simplifications must be imposed upon the atomic wave function used in the matrix element in Eq. (13) based on the realization that the role of the wave function here is mainly to introduce the appropriate atomic-length scale (or constriction diameter) into the problem. For the case of s states, the atomic orbitals are radial functions, $|A_s\rangle \rightarrow \psi_s(r)$, whereas p states are of the form $|A_p\rangle \rightarrow x_i \psi_p(r)$ with $x_i = x$, y, or z and, in both cases $\psi(r)$ is a spherically symmetric function whose mean radius is that of the relevant shell. It is very convenient to take the radial functions as Gaussians since both

$$\psi_s(r) = (2\alpha/\pi)^{3/4} \exp(-\alpha r^2) \quad (14a)$$

and

$$\psi_p(r) = (2\alpha/\pi)^{3/4} 2\alpha^{1/2} x_i \exp(-\alpha r^2) \quad (14b)$$

are in normalized product form; i.e.,

$$\psi(\mathbf{r}) = \prod_{i=1}^{3} \psi_i(x_i) \ .$$

With separable wave functions as specified by Eqs. (5) and (14), the modulus-squared tunneling matrix element of Eq. (13) becomes

$$|\langle F|O_T|A\rangle|^2 = |\langle \mathbf{k}_\parallel | \phi_\parallel \rangle|^2 |\langle f_z|O_z|\phi_z\rangle|^2 \ , \quad (15)$$

where $\langle \mathbf{k}_\parallel | \phi_\parallel \rangle$, the two-dimensional Fourier transform of the atomic function in the surface plane, is a measure of the transverse-momentum content of an electron passing through the a'th resonance state of the adatom and, as such, is the basis for "channel (or atomic excited-state) filtering." The term $|\langle f_z|O_z|\phi_z\rangle|^2$ is essentially the one-dimensional tunneling probability through that portion of the triangle barrier in Fig. 3 on the vacuum side of the adatom where $z > s + w_a$. The modulus-squared tunneling matrix element is identically

$$|\langle f_z|O_z|\phi_z\rangle|^2 = R |\langle f_z|O_z|m_z\rangle|^2 \ , \quad (16a)$$

with

$$R = |\langle f_z|O_z|\phi_z\rangle|^2 / |\langle f_z|O_z|m_z\rangle|^2 \ . \quad (16b)$$

In the spirit of the arguments used with Eqs. (8) and (10), the ratio of modulus-squared matrix elements and, thus, tunneling probabilities given by Eq. (16b) is

$$R = \exp\left[-2\int_{s+w_a}^{s_T} k(z) dz\right] / \exp\left[-2\int_0^{s_T} k(z) dz\right] \ ,$$

which, with $k(z)\simeq\kappa$ for the near-surface region $0<z<s$, simplifies to

$$R\simeq\exp[+2\kappa(s+w_a)]\ . \tag{17}$$

Thus, with Eqs. (10), (16), and (17), the z-dependent contribution to the tunneling probability is

$$4\pi^2\rho_f\rho_m|\langle f_z|O_z|\phi_{a,z}\rangle|^2\rightarrow\exp[2\kappa(s+w_a)]D_0(W)\ , \tag{18}$$

which can be further simplified with the "small-$(W\text{-}E_F)$ expression" for $D_0(W)$.[20]

The atomic-overlap integrals are easily evaluated using the Gaussian wave functions,[23] ultimately yielding the transverse-momentum distributions

$$|\langle\mathbf{k}_\parallel|\phi_s\rangle|^2=\gamma_s\exp\left[-\frac{4}{\pi}\bar{r}_{s,\parallel}^2k_\parallel^2\right] \tag{19a}$$

and

$$|\langle\mathbf{k}_\parallel|\phi_{p_x}\rangle|^2+|\langle\mathbf{k}_\parallel|\phi_{p_y}\rangle|^2=\gamma_pk_\parallel^2\exp(-\tfrac{1}{3}\bar{r}_{p,\parallel}^2k_\parallel^2)\ , \tag{19b}$$

where $2\bar{r}_{s,\parallel}=(\pi/2\alpha)^{1/2}$ is the mean diameter of the s shell, $2\bar{r}_{p,\parallel}=(3/2\alpha)^{1/2}$ is the rms diameter of the p_x/p_y shell, and the (unessential) numerical values for the proportionality constants in $\gamma_s=c_sr_\parallel^2$ and $\gamma_p=c_pr_\parallel^4$ depend upon normalization conventions, a point which will be returned to later. The long-wavelength or small-$k_\parallel$ cutoff in the p-wave resonance tunneling is a consequence of the nodal structure imposed upon the wave passing through the adatom via a p_x or p_y intermediate state.

B. Resonance energy distributions

To obtain explicit expressions from Eq. (13) for the total resonance field-emission current, the sum over final states must be carried out in order to pick up the influences of the "selection rules" imposed by adiabatic passage through the adatom. Without belaboring the point, note that in analogy with Eq. (9), the total resonance current given by Eqs. (13) and (15)–(17) is

$$j_{\rm res}=(4\pi e/\hbar)\sum_{a,\mathbf{k}_\parallel}\int_{-\infty}^{\infty}d\epsilon_f f(\epsilon_f)\rho_f\rho_a(\epsilon_f)\times|\langle\mathbf{k}_\parallel|\phi_\parallel\rangle|^2R|\langle f_z|O_z|m_z\rangle|^2\ . \tag{20}$$

Again using Harrison's WKB matrix element, Eq. (10), the total-energy distribution inferred from Eq. (20) is

$$dj_{\rm res}/d\epsilon_f=(e/\pi\hbar)f(\epsilon_f)\sum_{a,\mathbf{k}_\parallel}D_0(W)|\langle\mathbf{k}_\parallel|\phi_\parallel\rangle|^2\times\{[\rho_a(\epsilon_f)/\rho_m]\times\exp[2\kappa(s+w_a)]\}\ . \tag{21}$$

Converting the $\mathbf{k}_\parallel$ sum into a normal energy integral, as with Eq. (11), allows Eq. (21) to be written

$$dj_{\rm res}/d\epsilon_f=(4\pi me/h^3)f(\epsilon_f)\times\sum_a[\rho_a(\epsilon_f)/\rho_m]\times\int_0^{\epsilon_f}dW\,D_0(W)|\langle\mathbf{k}_\parallel|\phi_\parallel\rangle|^2\times\exp[2\kappa(s+w_a)]\ , \tag{22}$$

which can be nicely reduced for some important examples by using the linearized exponential form for $D_0(W)$. Since we are considering cases in which there is a large resonant enhancement in the field-emission current, the ratio considered in Eq. (2) is well represented as

$$\Delta j'(\epsilon_f)/j_0'(\epsilon_f)\simeq(dj_{\rm res}/d\epsilon_f)/(dj_0/d\epsilon_f) \tag{23}$$

using Eqs. (1) and (22) for the denominator and numerator, respectively. We now proceed to the specific cases.

(i) $k_\parallel\ll1/r,\kappa$ slowly varying. Two simplifications are possible in Eq. (22) due to the fact that $D_0(W)$ is large only within a few multiples of d (the barrier penetration decay constant) below E_F. This implies that over the limited range of W of significance in the Eq. (22) integral, not only is $k_\parallel$ very small but also κ is nearly constant. Consequently, the exponential is $\simeq\exp[2\kappa(\epsilon_f)(s+w_a)]$ and can be pulled out of the integral. Furthermore, when $k_\parallel r_\parallel\ll1$ (as it is when $\hbar^2k_\parallel^2/2m<d\approx0.1$ eV and $r_\parallel$ is a typical atomic-orbital radius) then, from Eq. (19a) the $k_\parallel$-overlap integral for an s-wave resonance is well approximated as a constant $\simeq\gamma_s$ whose value depends only on the normalization and is here set equal to one. With these simplifications, Eq. (22) reduces to

$$dj_{\rm res}/d\epsilon_f=(J_0/d)f(\epsilon_f)\exp(\epsilon_f/d)\times\sum_a[\rho_a(\epsilon_f)/\rho_m]\exp[2\kappa(s+w_a)]\ , \tag{24}$$

which, when combined with Eqs. (1) and (23), yields precisely Eq. (2), the long-standing resonance tunneling expression.

(ii) κ slowly varying, s resonance. If Eq. (19a), the full s-wave Gaussian expression for the transverse-momentum distribution, is retained in Eq. (22), then it is straightforward to show that, upon integration, the s-wave resonance tunneling expression can be brought to the form

$$\Delta j_s'(\epsilon_f)/j_0'(\epsilon_f)=c_s[r_{s,\parallel}^2/(1+\xi_sdr_{s,\parallel}^2)]\times\sum_a[\rho_a(\epsilon_f)/\rho_m]\exp[2\kappa(s+w_a)]\ , \tag{25}$$

where $\xi_s\equiv4(2m/\hbar^2)/\pi=0.33/\text{eV/Å}^2$ and c_s is purely numerical factor of order unity which is independent of system parameters. The dependence of $\Delta j_s'/j_0'$ on $r_\parallel$, the characteristic size of the resonance orbital (or constriction) is through the sigmoidal function $f_{s,\parallel}\equiv\xi_sdr_{s,\parallel}^2/(1+\xi_sdr_{s,\parallel}^2)$, which achieves a half-maximum value at $r_{s,\parallel}(\frac{1}{2})=(\xi_sd)^{-1/2}=1.73\phi^{1/4}/F^{1/2}$ Å, with ϕ in eV and F in V/Å, as shown in the normalized plot in Fig. 4(a). The physical implications of these results are interesting. For the smallest atom or aperture

size, the resonance tunneling current *density* approaches zero relative to the clean surface result. This follows since a tunneling electron must have a transverse wavelength that is comparable with the orbital size in order to pass through the constriction/atom. However, with a large amount of the total energy ($\leq E_F$) partitioned into transverse energy, there is little normal energy left for tunnel barrier penetration. As the size of the orbital increases, electrons with larger transverse wavelengths, hence, reduced transverse energies, are acceptable resonant-tunneling candidates. These electrons have larger normal energies and thus larger tunneling probabilities, resulting in enhanced resonant tunneling. Ultimately, the orbital size becomes sufficiently large [$r_{s,\parallel}(\frac{1}{2})\sim 5$ Å] for field-emission operating conditions) that the transverse-wavelength constraints no longer influence the tunneling characteristics and thus $\Delta j_s'/j_0'$ attains an $r_\parallel$-independent saturation.

(iii) κ slowly varying; p_x/p_y resonance. Using Eq. (19b), the full p_x/p_y Gaussian expressions for the transverse momentum in Eq. (22), one can show that the resulting tunneling expression is similar to Eq. (25) but with the multiplicative $r_{p,\parallel}$-dependent rescaling factor given as $f_{p,\parallel}=\xi_p^2 d^2 r_{p,\parallel}^4/(1+\xi_p d r_{p,\parallel}^2)^2$, where $\xi_p=(2m/\hbar^2)/3=0.087/\text{eV/Å}^2$. The half-maximum value of $f_{p,\parallel}$, shown as the normalized curves in Fig. 4(b), is achieved at

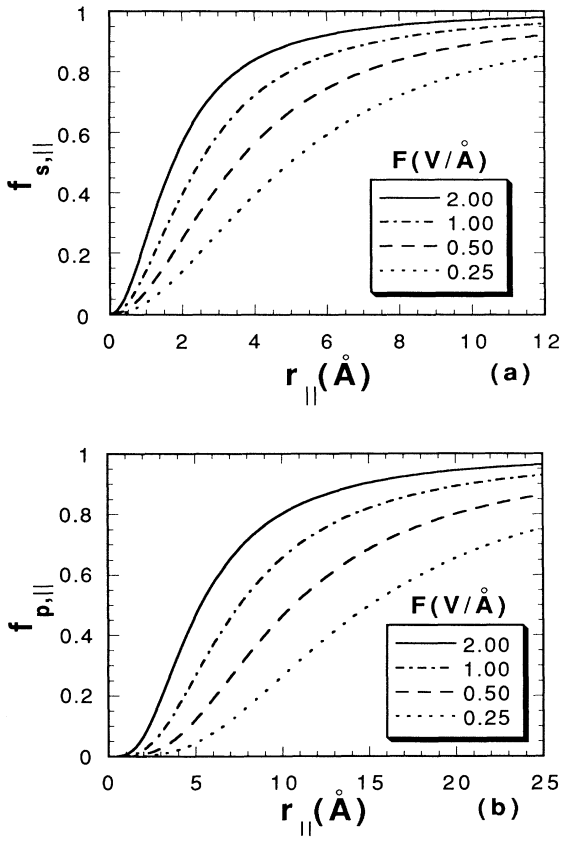

FIG. 4. (a) *s*-orbital/constriction size dependence of normalized change in the field-emission TED, from Eq. (25), varying ϕ and F as labeled. (b) Same as (a), but for $p_{x/y}$ resonance.

$r_{p,\parallel}(\frac{1}{2})=1.55(\xi_p d)^{-1/2}\sim 5.3\phi^{1/4}/F^{1/2}$ Å, which is much greater than the half-maximum radius for *s*-wave resonance. The physical origin of this consequence is also interesting and related to some aspects of "mode-number conservation" for a wave moving adiabatically along an electronic waveguide, as discussed by Lang, Yacoby, and Imry.[2] Put very simply, if an electron is to pass through a $p_\parallel$- rather than *s*- or p_z-orbital resonance, then since an additional node in the transverse component of the resonance-state wave function occurs, the tunneling electron must arrive with a finite $k_\parallel$, as implied by Eq. (19b). But this requirement takes even more away from the normal energy needed to penetrate the tunnel barrier than for the nodeless *s* resonance, hence the additional suppression of the resonance-assisted tunneling current relative to the *s*-state process, as is apparent in Fig. 4, for $r_\parallel$ small. The tunneling characteristics become independent of orbital or hole size only as the energy associated with the transverse momentum needed to project onto the $p_\parallel$ orbital becomes $<d$, the characteristic energy for barrier penetration. It is not unreasonable to imagine that this transition occurs when the wavelengths of the transverse motion and the orbital diameter are comparable, i.e., $\lambda_\parallel\sim 2r_\parallel$. Requiring that the associated energy equal d, the resulting orbital size is $r_\parallel=(\hbar^2\pi^2/2md)^{1/2}=6.24\phi^{1/4}/F^{1/2}$ Å which, for all practical purposes, is identical with $r_{p,\parallel}(\frac{1}{2})$ obtained from the full theory. The consequences of the transverse-momentum filtering have profound implications with respect to the angular distributions of the field-emission resonance tunneling.

C. Angular distributions

Finally, the issue of electron-beam collimation resulting from resonance tunneling through single atoms or adiabatic constrictions can be addressed. The connections between emitted electron-beam angular profiles and the atomic level-system properties is made clear by rewriting Eq. (21) as

$$dj_{\text{res}}/d\epsilon_f=\sum_a F_a(\epsilon_f)\sum_{\mathbf{k}_\parallel} D_0(W)|\langle \mathbf{k}_\parallel|\phi_{a,\parallel}\rangle|^2 , \quad (26)$$

where the expression for $F_a(\epsilon_f)$ is easily deduced by comparison with Eq. (21). Replacing the $\mathbf{k}_\parallel$ sum with an integral,

$$\sum_{\mathbf{k}_\parallel}\Longrightarrow\int\frac{d^2k_\parallel}{(2\pi)^2}$$

and converting to spherical coordinates in which $k_\parallel=k\sin\theta$, hence $d^2k_\parallel=k_\parallel dk_\parallel d\phi=k^2\cos\theta\sin\theta\, d\theta d\phi$, the angle-resolved energy distribution for the a'th resonance is

$$d^2j_{a,\text{res}}/d\Omega d\epsilon_f=\frac{F_a(\epsilon_f)k^2\cos\theta}{4\pi^2}D_0(\epsilon_f,\theta)|\langle \mathbf{k}_\parallel|\phi_{a,\parallel}\rangle|^2$$

$$\equiv j_a''(\epsilon_f,\theta) , \quad (27)$$

where $D_0(W)=D_0(\epsilon_f,\theta)=\exp(-c-E_F/d)\exp[(\epsilon_f/d)\cos^2\theta]$ and ϵ_f is the total kinetic energy of the electron

at the location of the "detector" which, for present purposes, will be imagined to be in the plane parallel to the surface at a distance $z=(\phi+E_F)/eF$ where the external electrostatic potential equals the inner potential of the emitter. As noted by Lang, Yacoby, and Imry,[2] using a large but still atomic-scale distance (with $F=1.3$ V/A, they used 30 bohr, typical STM-scale dimensions) allows one to concentrate on the microscopic aspects of beam collimation due to the tunneling process, unobscured by macroscopic field-focusing effects.

First consider the beam profile for s-resonance emission where the transverse-momentum distribution is given by Eq. (19a). It is convenient to work with the angular distribution normalized to the value at the angle of maximum emission which, for the s-resonance, is $\theta=0$, the surface normal direction. The resulting profile that follows from Eqs. (19a) and (27) is

$$R_S(\theta)\equiv j_S''(\theta)/j_S''(\theta=0) = \cos\theta\exp[(\epsilon_f/d)(\cos^2\theta-1)] \times\exp(-\xi_S r_{S,\parallel}^2\epsilon_f\sin^2\theta) \quad (28a)$$

which, in the reasonable small-θ limit ($\cos\theta\sim1$, $\sin\theta\sim\theta$), is simply

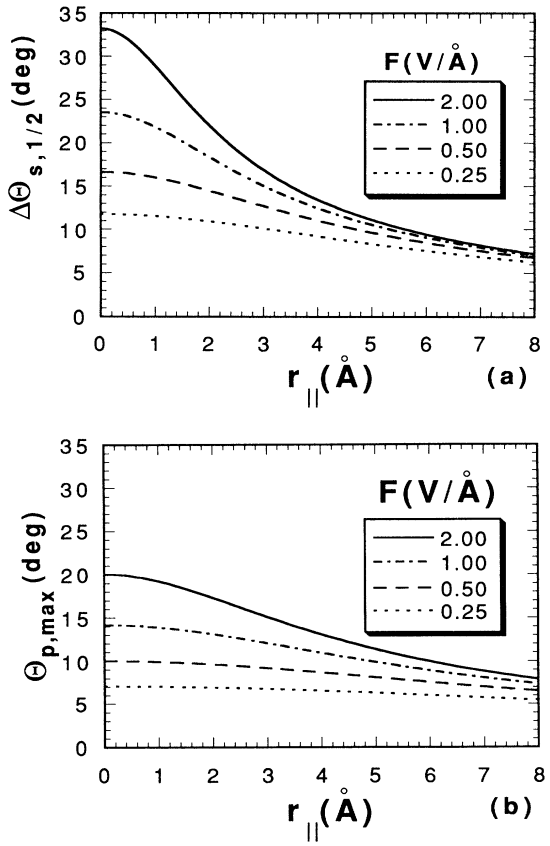

FIG. 5. (a) s-orbital/constriction size dependence of the beam-width $\frac{1}{2}$-angle attained on the $z=(\phi+E_F)/eF$ plane, varying F within the "typical" field emission and STM range. (b) $p_{x/y}$-orbital size dependence of beam maximum angle, for conditions as in (a).

$$R_S(\theta)\approx\exp(-\eta_S\theta^2)\ , \quad (28b)$$

with $\eta_s\equiv(1/d+\xi_s r_{s,\parallel}^2)\epsilon_f$. The emission profile is thus a normally directed Gaussian with a full width at half maximum given by

$$\Delta\theta_{S,1/2}=1.66/\eta_S^{1/2}\ . \quad (29)$$

The beam width as a function of orbital size, obtained from Eqs. (28) and (29), is shown in Fig. 5(a) for a range of field strengths appropriate to field emission and the STM. For field strengths typical of a FEM, $\Delta\theta_{s,1/2}$ shows a fairly weak dependence on orbital/aperture size, with the beam narrowing a little as the orbital radius increases. The effect is much more pronounced for STM-magnitude fields. This observation merits some further clarification. Certainly as $r_{s,\parallel}$ increases, so does the maximum permissible wavelength associated with the transverse momentum of the resonantly tunneling electron, hence the transverse momentum decreases and the beam sharpens. At the same time, the current density increases as already demonstrated through Eq. (25) and Fig. 4(a). However, as $r_{s,\parallel}$ increases, the conditions for "freezing out" the higher angular-momentum orbitals (with additional transverse nodes) are relaxed and these additional resonance channels should be considered. For instance, the beam profile for a $p_{x/y}$ resonance, from Eqs. (19b) and (27), is $j_p''(\theta)\propto\cos\theta\sin^2\theta\exp(-\eta_p\sin^2\theta)$, a halo profile with zero normal emission, maximum emission in the direction $\theta_{\max}\approx1/\eta_p^{1/2}$, and with full width at half maximum given by $\Delta\theta_{p,1/2}=1.16/\eta_p^{1/2}$. The beam angle thus obtained is shown in Fig. 5(b), as a function of orbital size, also for various field strengths. The dependence upon $r_{p,\parallel}$ is even weaker than for the s-orbital resonance, at least within the range of realistic atomic orbital sizes associated with the low-lying electronic states of candidate atomic species. Nonetheless, angle-dependent electron-beam production due to p-orbital resonance enhancement is expected to show characteristics that are noticeably different from resonance tunneling via s-orbital intermediate states. In both cases, however, the results are in accord with expectations based on the numerical studies of Lang, Yacoby, and Imry,[2] as applied within the context of an STM.

IV. FINAL REMARKS

A theory of field-emission resonance tunneling has been presented here which is a fully developed version of the original theory used more than twenty years ago in conjunction with pioneering experimental electron-spectroscopy studies of single adsorbed atoms.[5] For those adsorbates with virtual electronic states energetically near the substrate Fermi level, tremendous enhancements in the single-atom tunneling current density are both expected and observed.[6] Furthermore, the electron beam emerging from the single atom is expected to be highly collimated in a predictable field-dependent manner as a result of the microscopic tunneling process; this result is independent of any macroscopic field-focusing electron optics. The collimated electron beam can be realized experimentally both with ultrasharp tips ending

with one atom, as proposed by Fink and co-workers[1] as well as with a probe-hole field-emission microscope operating in a resonant tunneling mode, using single atoms adsorbed on the field-emission tip.[5–7]

The theory developed here applies equally well to tunneling phenomena in scanning-tunneling microscopes as discussed by Lang, Yacoby, and Imry,[2] in the most straightforward way by simply replacing the word "adatom" with "STM tip" throughout this paper. The simple analytic description provided here should serve as a useful complement to numerical simulations, particularly for quick insights into the relationships between observables in tunneling/conduction processes through atoms and/or narrow channels and the electronic properties of the individual constituents of the tunneling system.

ACKNOWLEDGMENTS

I acknowledge past collaborations with Ward Plummer and Russ Young at NBS/NIST on the topic of FERT, and also more recent discussions with Bob Celotta, Norton Lang, and Joe Stroscio on STM issues.

[1]H. W. Fink, Phys. Scr. **38**, 260 (1988); H. W. Fink, W. Stocker, and H. Schmid, Phys. Rev. Lett. **65**, 1204 (1990).

[2]N. D. Lang, A. Yacoby, and Y. Imry, Phys. Rev. Lett. **63**, 1499 (1989).

[3]N. D. Lang, Phys. Rev. B **36**, 8173 (1987).

[4]C. B. Duke and M. E. Alferieff, J. Chem. Phys. **46**, 923 (1967).

[5](a) H. E. Clark and R. D. Young, Surf. Sci. **12**, 385 (1968); (b) E. W. Plummer, J. W. Gadzuk, and R. D. Young, Solid State Commun. **7**, 487 (1969).

[6]J. W. Gadzuk and E. W. Plummer, Rev. Mod. Phys. **45**, 487 (1973).

[7](a) M. E. Lin, R. P. Andres, and R. Reifenberger, Phys. Rev. Lett. **67**, 477 (1991). (b) Vu Thien Binh, S. T. Purcell, N. Garcia, and J. Duglioni, *ibid.* **69**, 2527 (1992).

[8]S. Lundqvist, Phys. Scr. **38**, 233 (1988).

[9]S. Flugge, *Practical Quantum Mechanics* (Springer-Verlag, New York, 1974), Vol. II, p. 105.

[10]J. Tersoff and D. R. Hamann, Phys. Rev. B **31**, 805 (1985); J. Tersoff, in *Scanning Tunneling Microscopy and Related Methods,* edited by R. J. Behm, N. Garcia, and H. Rohrer (Kluwer, Dordrecht, 1990), p. 77.

[11]R. D. Young, Phys. Rev. **113**, 110 (1959).

[12]For the image-corrected surface barrier, $1/d$ is to be multiplied by a weakly field-dependent factor ≈ 1.05, as tabulated in Ref. 6.

[13]While observations of the energy-level structure of adsorbed atoms were made with ionization neutralization spectroscopy based on the Auger effect [H. D. Hagstrum, Phys. Rev. **150**, 495 (1966)], ambiguities were present in the unfolding and the subsequent interpretation of the raw data of the inherently two-electron process. Furthermore, the studies were carried out on partial monolayer systems, not single adsorbed atoms.

[14]For field-emission examples see J. W. Gadzuk, Phys. Rev. B **1**, 2110 (1970); D. R. Penn, R. Gomer, and M. H. Cohen, *ibid.* **5**, 768 (1972); A. Modinos, *Field, Thermionic, and Secondary Electron Emission Spectroscopy* (Plenum, New York, 1984).

[15]Recently, attention has been focused on inelastic resonance tunneling, e.g., B. N. J. Persson, Phys. Scr. **38**, 282 (1988); N. S. Wingreen, K. W. Jacobsen, and J. W. Wilkins, Phys. Rev. B **40**, 11 834 (1989); J. W. Gadzuk, *ibid.* **44**, 13 466 (1991).

[16]An exception to this is the one-dimensional wave-matching approach used by Duke and Alferieff in Ref. 4.

[17]For instance, $O_T \Longrightarrow eFz$ in the tunneling and field-ionization theory of Oppenheimer [Phys. Rev. **31**, 66 (1928)], whereas $O_T \Longrightarrow i\hbar j_{\rm op}$ in the Bardeen transfer Hamiltonian theory [Phys. Rev. Lett. **6**, 57 (1961)]. Nonetheless, the two approaches are equivalent, as demonstrated by C. B. Duke, in *Tunneling in Solids* (Academic, New York, 1969), p. 208.

[18]W. A. Harrison, Phys. Rev. **123**, 85 (1961).

[19]E. L. Wolf, *Principles of Electron Tunneling Spectroscopy* (Oxford University Press, New York, 1985).

[20]Parenthetically, note that for the triangle barrier $V(z)=\Theta(z)(E_F+\phi-eFz)$, one easily finds that $D_0(W)\approx\exp\{-(4/3eF)(2m/\hbar^2)^{1/2}[\phi-(W-E_F)]^{3/2}\}$. Furthermore, with a "small-$(W\text{-}E_F)$ expansion" about E_F, $D_0(W)\approx\exp[-c+(W-E_F)/d]$ which has been used in Eq. (1).

[21]As used here, O_T also contains the field-independent electron transfer or hopping interactions responsible for the adsorption bond.

[22]P. J. Feibelman, Prog. Surf. Sci. **12**, 287 (1982).

[23]J. W. Gadzuk, Surf. Sci. **180**, 225 (1987).